Contrib Mineral Petrol (1990) 104:1–7

Contributions to Mineralogy and Petrology

Constraints on phase diagram topology for the system $CaO-MgO-SiO_2-CO_2-H_2O$

Volkmar Trommsdorff and James A.D. Connolly
Institut für Mineralogie und Petrographie, Eidgenössische Technische Hochschule, CH-8092 Zürich, Switzerland

Abstract. Published phase diagrams for the siliceous carbonate system $CaO-MgO-SiO_2-CO_2-H_2O$ are contradictory because of different estimates of the relative stability of magnesite. Experimental data on magnesite are too ambiguous to determine the validity of these estimates. Therefore, field evidence is used to select the correct phase diagram topology for siliceous carbonate and carbonate ultramafic rocks at pressures of about 2–5 kbar. The primary selection criterion is provided by the existence of the stable assemblage talc + dolomite + forsterite + tremolite + antigorite, which occurs in the Bergell contact aureole and Swiss Central Alps. Field evidence also is used to argue that the reaction magnesite + quartz = enstatite must occur at lower temperature than the reaction dolomite + quartz = diopside. T-X_{CO_2} and P_{CO_2}-T phase diagrams consistent with these observations are calculated from experimental and thermodynamic data. For antigorite ophicarbonate rocks, remarkable agreement is obtained between the spatial distribution of low variance mineral assemblages and the calculated diagrams.

Introduction

Phase relations in the system $CaO-MgO-SiO_2-CO_2-H_2O$ are essential for understanding the petrogenesis of siliceous carbonate rocks. However, recent phase diagrams for parts of this system (e.g., Chernosky et al. 1988 p. 312 or Evans and Guggenheim 1988 p. 266), calculated using the thermodynamic data base of Berman (1988), are in substantial conflict with the earlier diagrams of Johannes and Metz (1968), Skippen (1971, 1974), Skippen and Hutcheon (1974), and Trommsdorff and Evans (1977a), among others. This is illustrated in Fig. 1 which compares the T-X_{CO_2} diagrams for ophicarbonate rocks from Trommsdorff and Evans (1977a) and Chernosky et al. (1988). In the digram of Trommsdorff and Evans (Fig. 1b), equilibria involving magnesite are displaced in such a way as to result in smaller stability fields for magnesite bearing assemblages than are predicted with the diagram of Chernosky et al. (Fig. 1a), As a consequence of this, a large stability field for Tr + M (phase notation is summarized in Table 1) appears in Fig. 1a, but is absent in Fig. 1b. Similarly, the assemblage Do + Fo + Tc is stable in Fig. 1b, but is not stable in Fig. 1a. These discrepancies have prompted the reexamination of the ophicarbonate phase diagram undertaken here. It will be shown that these discrepancies are primarily due to magnesite bearing equilibria. Consequently, experimental constraints on the stability of magnesite are addressed here first.

Offprint requests to: V. Trommsdorff

Stability of magnesite

The high temperature stability of magnesite is limited by the $M = P$ reaction. This reaction is critical for extracting the thermodynamic properties of magnesite because the properties of both periclase and CO_2 (at least at low pressures < 8 kbar) are well known. The location of the $M = P$ equilibrium predicted using Berman's (1988) data base is shown by curve B in Fig. 2 (see also Berman 1988 p. 499). However, the phase diagrams of Chernosky et al. (1988) and Evans and Guggenheim (1988) can only be reproduced if the reference state (298.15 K, 1 bar) Gibbs free energy of formation of magnesite ($\Delta G_{f,\text{magnesite}}(P_r, T_r)$) reported by Berman (1988, value B in Table 2) is decreased by 780 J.[1] The decreased value for $\Delta G_{f,\text{magnesite}}(P_r, T_r)$ (value C in Table 2) shifts the $M = P$ equilibrium to higher temperatures indicated by curve C in Fig. 2. It is noteworthy, that Fig. 2 shows two sets of experiments which were not used in Berman's (1988) analysis, those of Johannes and Metz (1968) and those of Philipp and Girsperger (1989) and Philipp (1989). Neither of these calculated curves, B or C, is in good agreement with these low pressure experimental determinations of the $M = P$ equilibrium as shown in Fig. 2. The experiments of Philipp and Girsperger are of particular interest, because they used a volumetric method (see also Schramke et al. 1982) which permits monitoring of reaction progress at run conditions. Taking into account calibration error, Philipp and Girsperger's experiments locate a region of feasible equilibrium conditions which is shown by the stippled pattern in Fig. 2.

Philipp and Girsperger's (1989) and Johannes and Metz's (1968) data are marginally consistent with those of and Harker and Tuttle (1955) and inconsistent with curves B and C in Fig. 2. The origin of these inconsistencies is probably not due to Philipp and Girsperger's pressure-temperature calibration which is in excellent agreement with that of Schramke et al. (1982) for the brucite decomposition reaction. Instead, there is a strong possibility that the experimental discrepancies reflect quenching difficulties in the earlier experiments. For these reasons, value A in Table 2 is adopted here for $\Delta G_{f,\text{magnesite}}(P_r, T_r)$ to calculate phase diagrams for siliceous carbonate rocks. This value is the median of the feasi-

[1] Since the preparation of this paper, Chernosky and Berman (1989) have revised the thermodynamic parameters of magnesite consistent with the Berman (1988) data base. Their new preferred value for $G_{f,\text{magnesite}}(P_r, T_r)$ is −1030.709 kJ/mol, derived using the magnesite third law entropy of Hemingway et al. (1977) of 65.09 J/mol-K at 298.15 K and 1 bar. This value is essentially equivalent to value C in Table 2, and was apparently used to calculate the phase diagrams of Chernosky et al. (1988) and Evans and Guggenheim (1988).

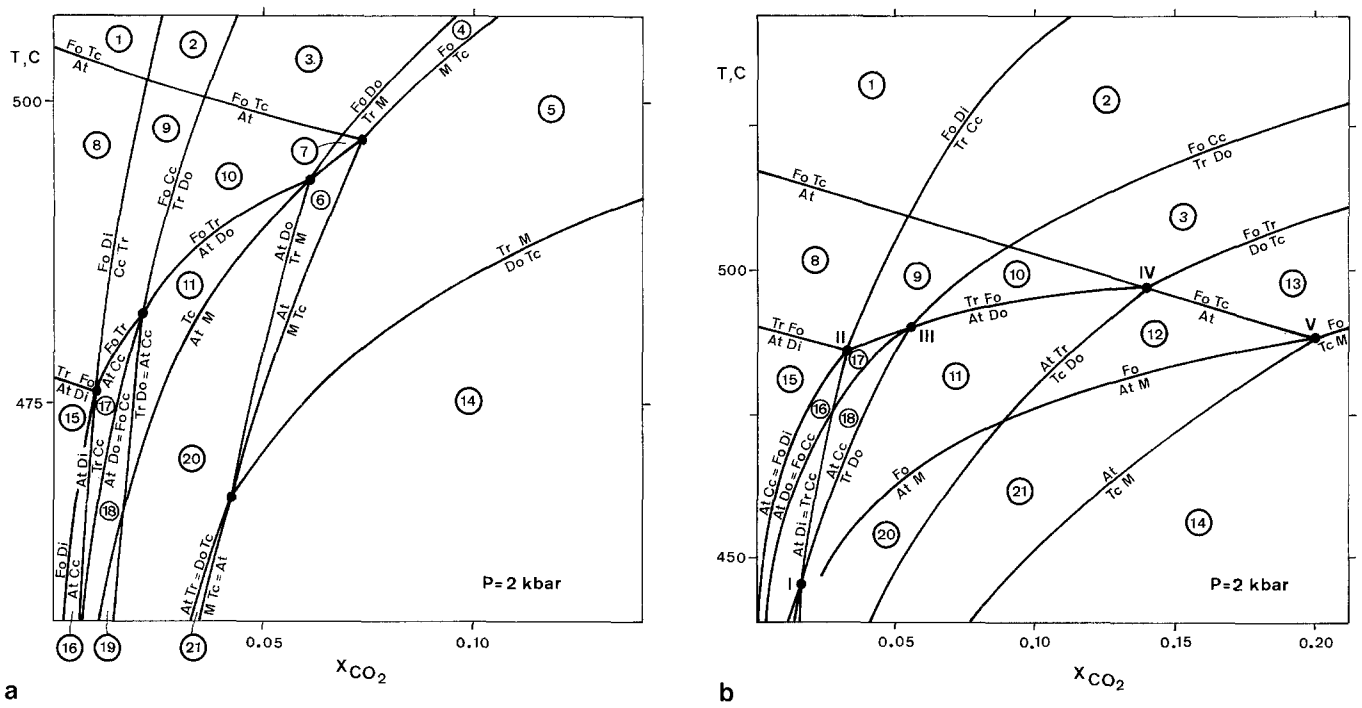

Fig. 1 a–c. T-X_{CO_2} diagrams at 2 kbar fluid pressure for antigorite-ophicarbonates (see Table 1 for phase notation). **a** Diagram of Chernosky et al. (1988) obtained using value C (Table 2) for $\Delta G_{f,\text{magnesite}}(P_r, T_r)$, together with Berman's (1988) data, and the HSMRK equation of state (Kerrick and Jacobs 1981). **b** Diagram of Trommsdorff and Evans (1977a). **c** Chemographic phase relationships in the numbered fields of Fig. **a** and **b**

Table 1. Phase notation and compositions

Symbol	Phase	Chemical Composition
At	Antigorite	$Mg_{48}Si_{34}O_{85}(OH)_{62}$
Ap	Anthophyllite	$Mg_7Si_8O_{22}(OH)_2$
Cc	Calcite	$CaCO_3$
Di	Diopside	$CaMgSi_2O_6$
Do	Dolomite	$CaMg(CO_3)_2$
E	Enstatite	$MgSiO_3$
Fo	Forsterite	Mg_2SiO_4
M	Magnesite	$MgCO_3$
P	Periclase	MgO
Q	Quartz	SiO_2
Tc	Talc	$Mg_3Si_4O_{10}(OH)_2$
Tr	Tremolite	$Ca_2Mg_5Si_8O_{22}(OH)_2$
Wo	Wollastonite	$CaSiO_3$

ble values for $\Delta G_{f,\text{magnesite}}(P_r, T_r)$, derived from Philipp and Girsperger's experiments by linear programming, that are consistent with Berman's (1988) entropy and volumetric functions (Philipp and Girsperger 1989). Curve A, in Fig. 2, defines the $M = P$ equilibrium conditions obtained for this value of $\Delta G_{f,\text{magnesite}}(P_r, T_r)$. This value for $\Delta G_{f,\text{magnesite}}(P_r, T_r)$ is also consistent with earlier experiments on high pressure magnesite bearing equilibria by several different investigators (Connolly et al. 1989).

Calculated phase diagrams for the system $CaO-MgO-SiO_2-CO_2-H_2O$

The two extreme values for $\Delta G_{f,\text{magnesite}}(P_r, T_r)$ in Table 2 have been used together with the thermodynamic data base of Berman (1988) to calculate isobaric T-X_{CO_2} phase diagrams for the fluid saturated system $CaO-MgO-SiO_2-CO_2-H_2O$ with the VERTEX computer program (Connolly and Kerrick 1986; Connolly 1989). Properties of the fluid phase have been calculated using the modified Redlich-Kwong-type equation of state developed by Kerrick and Jacobs (1981). To simplify the diagrams only the minerals Cc, Do, M, At, Tc, Ap, E, Fo, Di, Tr, and Q are considered. The stability of other minerals, with the exception of Wo (which forms from Cc+Q at low X_{CO_2}), would only alter the diagrams at extreme fluid compositions and temperatures.

Figure 3 shows a phase diagram calculated using value C (Table 1) for $\Delta G_{f,\text{magnesite}}(P_r, T_r)$ which yields curve C in Fig. 2. This diagram duplicates and extends the diagram published by Chernosky et al. (1988 p. 312, also Fig. 1b here). Figure 3 also reproduces the diagram of Evans and Guggenheim (1988 p. 266), but with the addition that diopside and calcite stability, which causes some of the equilibria in the Evans and Guggenheim diagram to be metastable, are taken into to account. Figure 4 is a phase diagram generated with a value for $\Delta G_{f,\text{magnesite}}(P_r, T_r)$ consistent with Philipp and Girsperger's (1989) experiments (value A in Table 2 and curve A in Fig. 2). The topology of Fig. 4 is identical to that of Trommsdorff and Evans (1977a) for ophicarbonate rocks which was calculated using experimentally derived equilibrium constant expressions from Skippen (1974) and from Evans et al. (1976). The major contradictions between the topologies of Figs. 3 and 4 are: (i) In Fig. 3, a large stability field for Tr+M (dotted region in Fig. 3) extends across almost the entire range of fluid compositions; whereas, in Fig. 4, Tr+M assemblages are restricted to a miniscule field compatible only with CO_2-rich fluids. As a consequence of this difference, the equilibrium Do+Tc=Fo+Tr, which is stable over a wide range of fluid compositions in Fig. 4, is precluded from Fig. 3 by the equilibrium Do+Tc=Tr+M. Thus, a stability field for the assemblage Do+Tc+Fo occurs in Fig. 4 (shaded re-

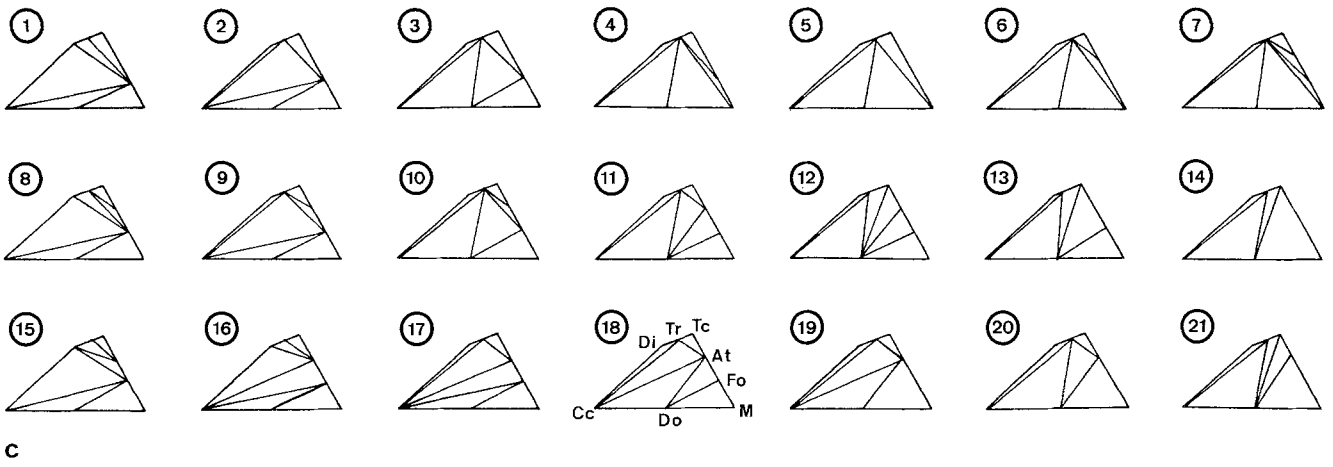

gion), and is absent in Fig. 3. (ii) The relative order of the reactions M+Q=E and Do+Q=Di is reversed in Figs. 3 and 4, resulting in Di+M stability only in Fig. 3 and E+Do stability only in Fig. 4.

There is an intermediate ophicarbonate phase diagram topology between the topologies of Figs. 3 and 4 (and Fig. 1a and b). This intermediate topology is obtained with the value for $\Delta G_{f,\text{magnesite}}(P_r, T_r)$ originally proposed by Berman (1988, value *B* in Table 2 here). In this topology, all the invariant point assemblages in Fig. 1a are stable, with the addition of a fifth invariant point representing the stability of the assemblage At+Tr+Do+Tc+M. The intermediate topology is obtained for values of $\Delta G_{f,\text{magnesite}}(P_r, T_r)$ ranging over about 1 kJ. Because this intermediate topology results in the same general features as Figs. 3 and 1a, it is not considered further here.

On the basis of Philipp and Girsperger's experiments (1989) alone, there is already some reason to favor the ophicarbonate phase diagrams shown in Fig. 4. However, field evidence, discussed in the following section, supports this choice.

Field constraints on the antigorite-ophicarbonate phase diagram

Uncertainty and inconsistency among the thermodynamic and experimental data for the $CaO-MgO-SiO_2-H_2O-CO_2$ system make an unequivocal choice between the topologies of Figs. 3 and 4 impossible without consideration of field evidence. Both topologies are consistent with the existence of the most common natural ophicarbonate assemblages in the Bergell aureole (Trommsdorff and Evans 1977a) At+Fo+Tr+Cc, At+Tr+Cc+Do, and At+Di+Tr+Cc, as noted by Chernosky et al. (1988). However, more thorough review of the literature reveals that the assemblage Tc+Do+Fo is not uncommon in the Bergell (Trommsdorff and Evans 1977b), and it has also been found in the Swiss Central Alps (Bosco-Gurin area). The stable occurrence of this assemblage, which is impossible given the topology of Fig. 3, is strong supporting evidence for selecting the topology of Fig. 4. The alternative assemblage Tr+M, which is stable in the phase diagram topology of Chernosky et al. (1988), has not been found at Bergell. To determine if pressure or mineral solutions could be responsible for stabilizing Tc+Do+Fo, or destabilizing Tr+M, at Bergell, these factors are considered below.

Table 2. Values for the reference state (298.15 K, 1 bar) Gibbs free energy of formation for magnesite from the elements ($\Delta G_{f,\text{magnesite}}[P_r, T_r]$) discussed in the text. These values are derived assuming a third law entropy of 65.21 J/mol-K for magnesite at reference state conditions. Value *A* is the value preferred here and was obtained from the experiments of Philipp and Girsperger (1989). Value *B* is the value reported in Berman (1988). Value *C* was estimated here to reproduce the phase diagrams of Chernosky et al. (1988) and Evans and Guggenheim (1988)

Value	$\Delta G_{f,\text{magnesite}}(P_r, T_r)$ (kj/mol)
A	−1027.436
B	−1029.875
C	−1030.655

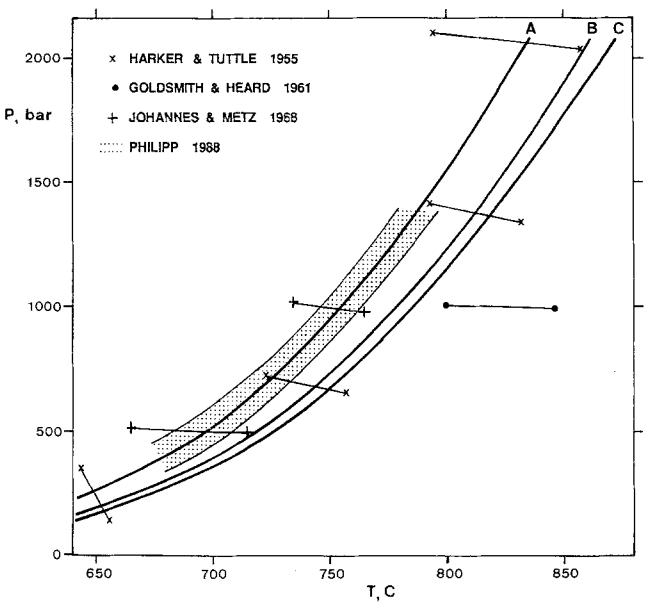

Fig. 2. Experimental constraints and calculated equilibrium conditions for the reaction $M=P+CO_2$. *Bracket symbols* are located taking into account the maximum experimental error estimated by the experimentalists. The *stippled region* locates the region of possible equilibrium conditions determined by Philipp and Girsperger's (1989) statistical analysis of their experiments. Three calculated equilibrium curves, *A*, *B* and *C*, are shown and correspond to the three values for $\Delta G_{f,\text{magnesite}}(P_r, T_r)$ given in Table 2. Curve *A* is preferred here

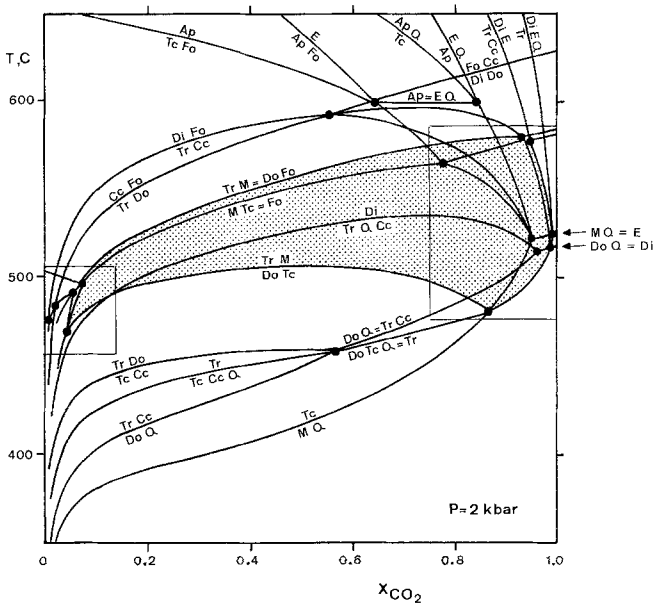

Fig. 3. T-X_{CO_2} diagram at 2 kbar fluid pressure for the system $CaO-MgO-SiO_2-H_2O-CO_2$ calculated using value C (Table 2) for $\Delta G_{f,\text{magnesite}}(P_r, T_r)$, together with Berman's (1988) data, and the HSMRK equation of state (Kerrick and Jacobs 1981). This diagram duplicates and extends those of Chernosky et al. (1988) and Evans and Guggenheim (1988). The *stippled area* defines the stability field of Tr + M assemblages. The *square* marks the conditions shown in Fig. 1a

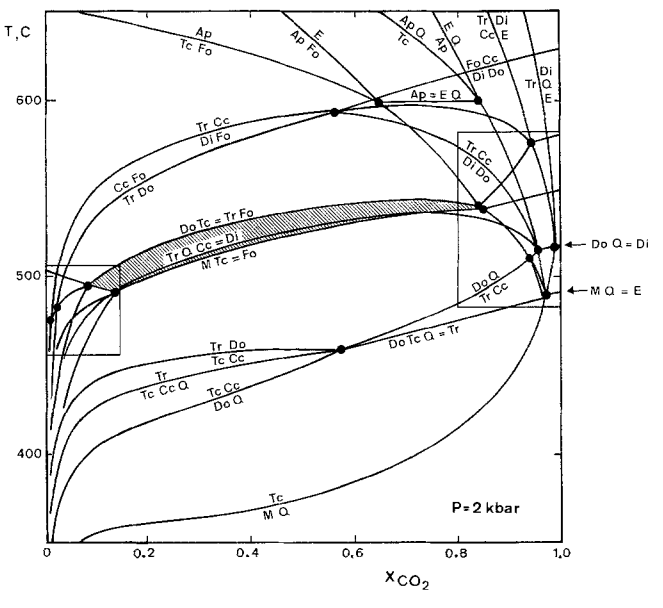

Fig. 4. Preferred T-X_{CO_2} diagram at 2 kbar fluid pressure for the system $CaO-MgO-SiO_2-H_2O-CO_2$ calculated using value A (Table 2) for $\Delta G_{f,\text{magnesite}}(P_r, T_r)$, together with Berman's (1988) data, and the HSMRK equation of state (Kerrick and Jacobs 1981). The *shaded area* indicates the stability field of Fo + Do + Tc. The *squares* delineate the region in which the ophicarbonate diagram topology of Figs. 1b and 5 is reproduced, and the high-X_{CO_2} region shown in detail in Fig. 7

Pressure estimates for the relevant part of the Bergell aureole range around 2.9–4.4 kbar on the basis of tectonic overburden (8–12 km, Cornelius 1925) and mineralogy (Carmichael 1978). Because these estimates are as much as 1.5 kbar higher than the pressure used to calculate Figs. 1, 3, and 4, the ophicarbonate phase diagrams in Figs. 3 and 4 were recalculated at 3.5 kbar. These higher pressure phase diagrams, though not shown here, are topologically equivalent to the 2 kbar diagrams of Figs. 3 and 4, but the stability field of Tr + M (in Fig. 3) is expanded and that of Tc + Do + Fo (in Fig. 4) is diminished. Pressure uncertainty at the Bergell, therefore, cannot be used as an argument to explain the stability of the phase diagram topology shown in Fig. 3.

To determine if the Bergell assemblage Tc + Do + Fo has been stabilized by solution effects, mineral compositions in a Bergell sample containing this assemblage have been determined by electron microprobe analysis. The only major impurity in the Bergell silicates is Fe^{2+}, so the silicate compositions may be expressed by X_{Mg} for which the following values were obtained: $X_{Mg,\text{olivine}} = 0.904$, $X_{Mg,\text{talc}} = 0.982$, and $X_{Mg,\text{antigorite}} = 0.953$. The composition of the dolomite coexisting with these silicates is $Ca_{0.977}Mg_{0.995}Fe_{0.024}Mn_{0.004}(CO_3)_2$. The Fe–Mg partitioning among these minerals is in excellent agreement with that of other metamorphic ultramafic assemblages both at Bergell and Val Malenco (Trommsdorff and Evans 1972). This agreement suggests that the observed assemblage was in exchange equilibrium. Because both tremolite and magnesite (Evans and Trommsdorff 1974) partition Fe^{2+} more strongly than either Do or Tc, the effect of iron solution is to stabilize Tr + M. As Tr + M is not observed at Bergell, mineral solution effects, like pressure, are not the source of the discrepancy between the topology of Fig. 3 and the observed mineral assemblages in the Bergell. Thus, the preponderance of evidence suggests that the topology of Figs. 1a and 3 are incorrect and that the topology of Figs. 1b and 4 are correct, at least for water-rich conditions.

The ophicarbonate phase diagrams of Trommsdorff and Evans (1977a, b), though topologically consistent with the observed phase assemblages at Bergell, fail to completely explain the spatial distribution of the assemblages (see Trommsdorff and Evans 1977b p. 309). This failing arises because in the phase diagrams of Trommsdorff and Evans (1977a, reproduced here as Fig. 1b, and 1977b) invariant point III occurs at higher temperature than invariant point V. However, in the Bergell aureole, the invariant point V assemblage occurs nearer the contact, and therefore presumably formed at higher temperature, than the assemblage corresponding to invariant point III. This difficulty disappears if the phase diagram in Fig. 4 is adopted in place of those used by Trommsdorff and Evans (1977a, b). In fact, the agreement between the spatial distribution of mineral assemblages at Bergell and the phase diagram consistent with Philipp and Girsperger's experiments (1989) is remarkably good, when activity corrections are applied, as shown by Fig. 5. This excellent agreeement suggests that if the value for $\Delta G_{f,\text{magnesite}}(P_r, T_r)$ is increased (to value A in Table 1), Berman's (1988) thermodynamic data base can be applied with some confidence for ophicarbonate minerals.

Field constraints on the carbonate ultramafic phase diagram

Unlike ophicarbonates, which are in equilibrium only with water-rich fluids, carbonate ultramafic rocks (e.g., sagvandites, see Schreyer et al. 1972) form in equilibrium with fluids of highly variable composition. Unfortunately, min-

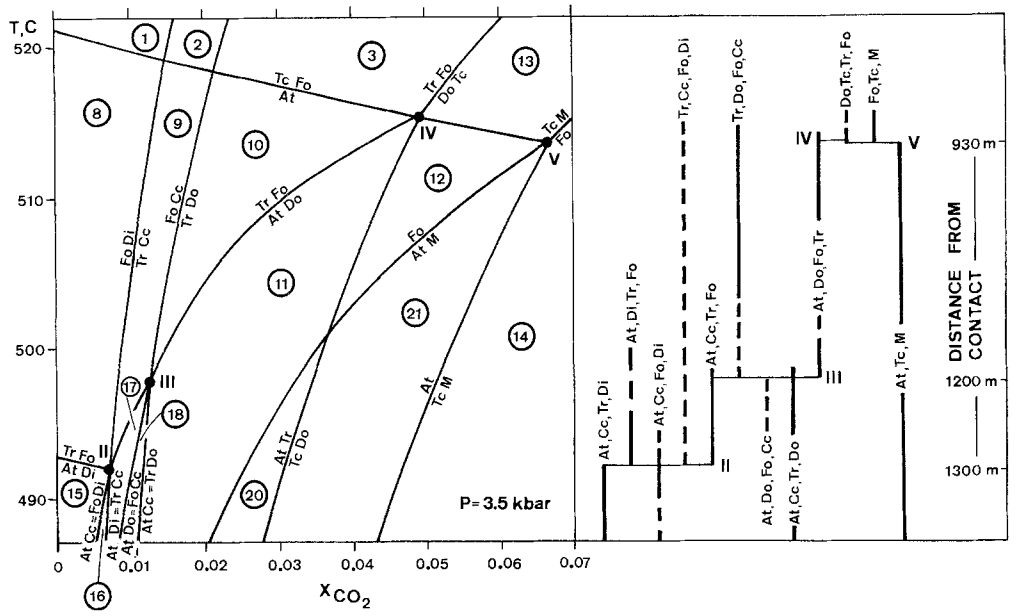

Fig. 5. Activity corrected T-X_{CO_2} diagram at 3.5 kbar fluid pressure for the system $CaO-MgO-SiO_2-H_2O-CO_2$ calculated using value *A* (Table 2) for $\Delta G_{f,\text{magnesite}}(P_r, T_r)$, together with Bermans' (1988) data, and the HSMRK equation of state (Kerrick and Jacobs 1981). Activity corrections were made assuming ideal solution models and the following Mg site fractions derived from the Fe–Mg distribution coefficients (Trommsdorff and Evans 1974): $X_{\text{Mg,anthophyllite}}=0.88$, $X_{\text{Mg,antigorite}}=0.95$, $X_{\text{Mg,diopside}}=0.965$, $X_{\text{Mg,enstatite}}=0.90$, $X_{\text{Mg,magnesite}}=0.89$, $X_{\text{Mg,olivine}}=0.89$, $X_{\text{Mg,talc}}=0.97$, and $X_{\text{Mg,tremolite}}=0.96$. Activity corrections were not made for Do or Cc because the corrections are small and introduce complexities which are beyond the scope of this paper. Invariant point labeling corresponds to that of Trommsdorff and Evans (1977a), the invariant assemblages are: II) Tr+Cc+At+Fo+Di, III) Tr+Cc+Do+Fo+At, IV) Tr+Fo+Do+Tc+At, and V) Tr+Fo+Do+Tc+At. On the *right hand side* of the diagram, the distribution of isobarically univariant and invariant assemblages in the Bergell aureole are shown as a function of their normal distance from the intrusive contact. *Dashed lines* and *solid lines* indicate, respectively, rare and common assemblages (see Trommsdorff and Evans 1977b)

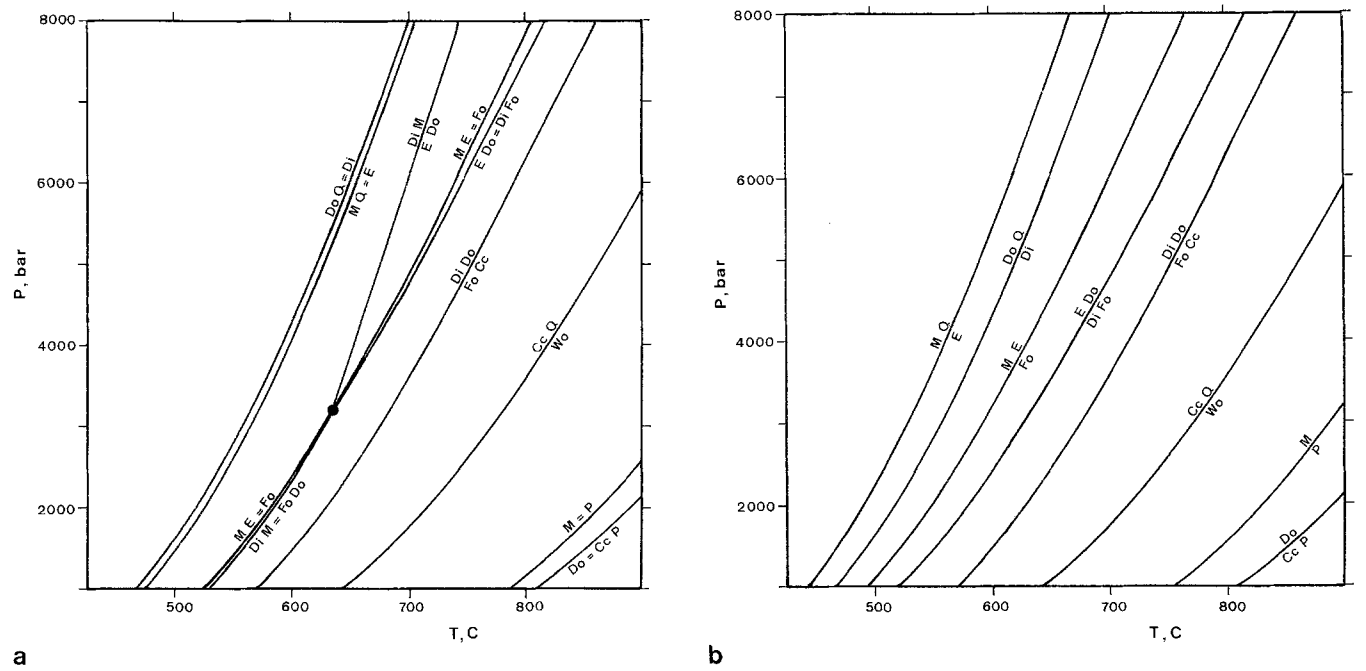

Fig. 6. **a** *P-T* diagram for the CO_2 saturated system $CaO-MgO-SiO_2$ calculated using value *C* (Table 2) for $\Delta G_{f,\text{magnesite}}(P_r, T_r)$, together with Berman's (1988) data, and the HSMRK equation of state (Kerrick and Jacobs 1981). **b** As **a** but $CaO-MgO-SiO_2$ calculated using value *A* (Table 2) for $\Delta G_{f,\text{magnesite}}(P_r, T_r)$. Diagram **b** is preferred here, note that in **a** the equilibrium of Do+Q=Di occurs at lower temperature than does M+Q=E resulting in a large stability field for Di+M assemblages

eral assemblages reported from field studies on carbonate ultramafic rocks are inadequate to uniquely determine the correct phase relations over the entire range of X_{CO_2} for the $CaO-MgO-SiO_2-H_2O-CO_2$ system. However, sufficient evidence exists to determine the sequence of decarbonation reactions for the anhydrous subsystem as a function of pressure and temperature. The phase diagrams calculated for this subsystem using the values of

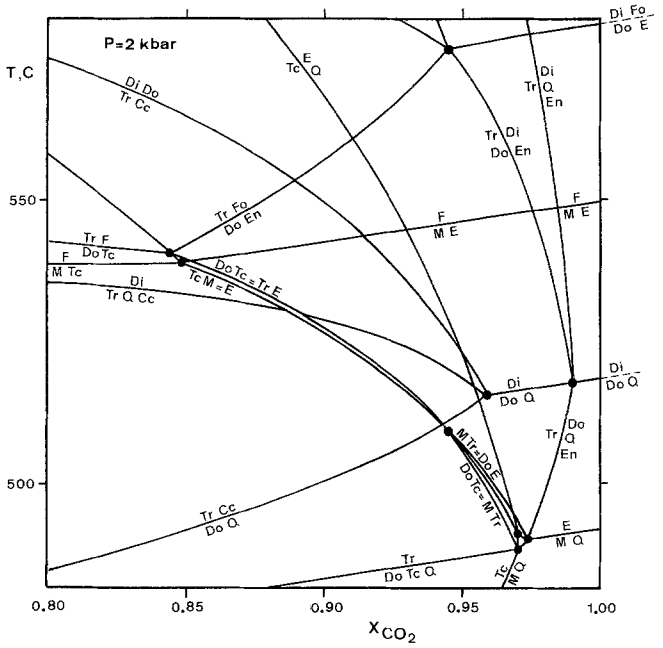

Fig. 7. Detail of the CO_2-rich portion of the T-X_{CO_2} diagram (Fig. 4) preferred here for the system $CaO-MgO-SiO_2-H_2O-CO_2$ at 2 kbar fluid pressure. Note the small stability field for Tr + M assemblages at high X_{CO_2}

$\Delta G_{f,\text{magnesite}}(P_r, T_r)$ consistent with Chernosky et al. (1989) and Philipp and Girsperger (1989), respectively, are shown in Fig. 6a and b. As previously mentioned, the most important difference between the two topologies in Fig. 6 is the relative order of the M + Q = E and Do + Q = Di equilibria, as governed by the fluid-absent equilibrium Di + M = E + Do. This inversion produces a stability field for M + Di assemblages over a substantial temperature interval in the diagram shown in Fig. 6a. Additionally, it is apparent that the stable reactions, and their sequence, in the diagram consistent with Chernosky et al. (1988, Fig. 6a) are pressure dependent. As a result of this pressure dependence, the assemblage Do + E would be metastable at pressures below 3 kbar. In the phase diagram topology calculated from Philipp and Girsperger's (1989) experiments (Fig. 6b), Do + E is stable at all pressures and M + Di is always metastable.

The assemblage Do + E is not an uncommon natural assemblage (Schreyer et al. 1972), and has been shown to be stable at 2 kbar by the experiments of Skippen (1971). Do + E is only stabilized at pressures above 3 kbar in the phase diagram Fig. 6a consistent with Chernosky et al. (1988). Although this is inconsistent with the experiments of Skippen (1971), it does not, in itself, preclude the topology of Fig. 6a. However, the absence of Di + M in all metamorphic sequences of ultramafic-carbonate assemblages so far observed (Schreyer et al. 1972; Trommsdorff and Evans 1974, 1977b; Ohnmacht 1974; Pfeifer 1979; Bucher-Nurminen 1988) is a strong, though negative, argument against the topology of Fig. 6a. By far the most compelling evidence for rejecting the topology of Fig. 6a in favor of the topology of Fig. 6b, is the order of appearance of E + M and Di + Do with increasing grade in the Central Alps (Figs. 8 and 9 in Trommsdorff and Evans 1974, and Fig. 1 in Trommsdorff 1972). This order can only be reconciled with the topology of Fig. 6b. Thus, field observations provide almost unequivocal evidence supporting the validity of the phase diagram topology (Fig. 6b) calculated using the $\Delta G_{f,\text{magnesite}}(P_r, T_r)$ derived from Philipp and Girsperger's experiments (1989).

Figure 7 shows the details of the CO_2-rich portion of the T-X_{CO_2} phase diagram preferred here (Fig. 4) for the $CaO-MgO-SiO_2-H_2O-CO_2$ system at low pressures. A point of interest in this diagram is the small stability field of Tr + M at CO_2-rich conditions. This field expands with pressure, explaining the occurrence of Tr + M assemblages in high pressure terrains (Schreyer et al. 1972; Pfeiffer 1979; Evans and Trommsdorff 1983; Bucher-Nurminen 1988). Although the topology of Fig. 7 is supported by field evidence in the limits of H_2O-rich and CO_2-rich fluid compositions, it should be regarded as tentative until verified by direct field evidence.

Conclusion

Uncertainties in experiments and data analysis are generally too large to permit direct, uncritical, thermodynamic calculation of geologic phase diagrams. For example, variation in the Gibbs free energy of magnesite, over a range of less than 1 kJ/mole, results in three different T-X_{CO_2} phase diagram topologies for ophicarbonates, and even more topologies if less water-rich conditions are considered. The ambiguity resulting from this is apparent from differences in calculated phase diagrams for the $CaO-MgO-SiO_2-H_2O-CO_2$ system (e.g., Trommsdorff and Evans 1977a; Chernosky et al. 1988; Evans and Guggenheim 1988). For this system, the ambiguity has been resolved here on the basis the of evidence from ophicarbonate and carbonate ultramafic mineral assemblages. The occurrence of the ophicarbonate assemblages, in particular Do + Tc + Fo, can only be explained with the phase diagram topology originally obtained by Trommsdorff and Evans (1977a, Figs. 1b, 4, and 5, here). Moreover, in the alternative topologies, the large stability field for Tr + M does not appear to be realized in natural low-pressure water-rich environments. At more CO_2-rich conditions, relevant for carbonate ultramafics, field evidence suggests that the phase diagram of Evans and Guggenheim (1988), which extends the diagram of Chernosky et al. (1988), is incorrect. In this diagram the M + Q = E equilibrium occurs at higher temperature than does the Do + Q = Di equilibrium, with the consequence that a large stability field for Di + M assemblages is created. An alternative phase diagram has been presented here (Figs. 4 and 6) which is in agreement with both field and experimental evidence.

The analysis presented here demonstrates the importance of using field evidence in conjunction with thermodynamic data to derive geologically meaningful phase diagrams. In the present case, field evidence has been used to argue that the Gibbs free energy of magnesite must be increased relative to other phases in the thermodynamic data base of Berman (1988). This increase is supported by recent experiments in which the reaction $P = M$ was monitored at run conditions (Philipp and Girsperger 1989), and by the earlier phase equilibrium experiments of Johannes and Metz (1968). The phase diagram calibration obtained with the increased magnesite Gibbs free energy, together with Berman's data (1988), shows remarkable agreement with the spatial distribution of mineral assemblages in the Bergell aureole (Fig. 5). Although this calibration appears satisfactory, other thermodynamic data bases (e.g., Helge-

son et al. 1978) produce, without modification, phase diagrams which are topologically consistent with field observations. Fluid composition (X_{CO_2}) is by far the most uncertain parameter of this calibration. The present calibration was obtained using fluid equation of state of Kerrick and Jacobs (1981). Alternative equations of state, such as the MRK equation popularized by Holloway (1977), which may be more reliable for mixed volatile fluids at low temperature, shift phase fields to more extreme values of X_{CO_2}. Thus, caution should be applied in attempts to quantify the composition of the fluids in equilibrium with siliceous carbonates. In addition, dilute salt components may introduce complications in the phase relations of metamorphosed carbonate rocks (Skippen and Trommsdorff 1986). In the case of the Malenco ophiolites, salt concentrations appear to have been extremely low (Peretti 1989) which may explain the excellent agreement between the distribution of ophicarbonate assemblages from the Bergell aureole and the calculated phase diagram of Fig. 6.

Acknowledgements. We would like to express our gratitude to Peter Ulmer for microprobe analyses, to Brigitte Bühlmann for excellent drafting, and to Claudia Büchel for typing. This paper was improved by the thorough reviews of Bernard Evans and George Skippen. Financial support from Schweizerischer National Fonds grants 2000-5.240 and 2000.5-493 and computer fonds from The University of Zürich is also gratefully acknowledged.

References

Berman RG (1988) Internally consistent thermodynamic data for minerals in the system $Na_2O-K_2O-CaO-MgO-FeO-Fe_2O_3-SiO_2-TiO_2-H_2O-CO_2$. J Petrol 29:445–552

Bucher-Nurminen K (1988) Metamorphism of ultramafic rocks in the central Scandinavian Caledomides. Nor Geol Unders Spec Publ 31:86–95

Carmichael DM (1978) Metamorphic bathozones and bathograds: a measure of the depth of post-metamorphic uplift and erosion on the regional scale. Am J Sci 278:769–797

Chernosky JV, Berman RG, Bryndzia LT (1988) Stability, phase relations and thermodynamic properties of chlorite and serpentine group minerals. Rev Mineral 19:295–346

Chernosky JV, Berman RG (1989) Experimental reversal of the equilibrium: clinochlore + 2 magnesite = 3 forsterite + spinel + 2 CO_2 + 4 H_2O and revised thermodynamic properties for magnesite. Am J Sci 289:249–266

Connolly JAD (1989) Calculation of multivariable phase diagrams: a computer strategy based on generalized thermodynamics. Am J Sci (in review)

Connolly JAD, Kerrick DM (1987) An algorithm and computer program for calculating computer phase diagrams. CALPHAD 11:1–55

Connolly JAD, Trommsdorff V, Philipp R (1989) A revised Gibbs free energy for Magnesite. Am J Sci (in review)

Cornelius HP (1925) Über einige Gesteine der ‚Fedozserie' aus dem Disgraziagebiet (Rhaetische Alpen). N Jahrb Mineral Beil Bd LII Abt A:1–50

Evans BW, Guggenheim S (1988) Talc, pyrophyllite and related minerals. Rev Mineral 19:225–294

Evans BW, Trommsdorff V (1974) Stability of enstatite + talc and CO_2-metasomatism of metaperidotite, Val d'Efra, Lepontine Alps Am J Sci 274:274–296

Evans BW, Trommsdorff V (1983) Flourine hydroxyl titanian clinohumite in alpine recrystalized peridotite: compositional controls and petrologic significance. Am J Sci 283-A:355–369

Evans BW, Johannes W, Oterdoom H, Trommsdorff V (1976) Stability of chrysotile and antigorite in the serpentine multisystem. Schweiz Mineral Petrogr Mitt 56:79–93

Goldsmith JR, Heard HC (1961) Subsolidus phase relations in the system $CaCO_3-MgCO_3$. J Geol 69:45–74

Harker RI, Tuttle OF (1955) Studies in the system $CaO-MgO-CO_2$, Part I: The thermal dissociation of calcite, dolomite and magnesite. Am J Sci 253:209–224

Helgeson HC, Delany JM, Nesbitt HW, Bird DK (1978) Summary and critique of the thermodynamic properties of rock-forming minerals. Am J Sci 278-A:1–229

Hemingway BS, Robie RA, Fisher JR, Wilson JH (1977) The heat capacities of Gibbsite, $Al(OH)_3$, between 13 and 480 K and Magnesite, $MgCO_3$, between 13 and 380 K and their standard entropies at 298.15 K and the heat capacities of Calorimetry Conference Benzoic Acid between 12 and 316 K. US Geol J Res 5:797–806

Holloway JR (1977) Fugacity and activity of molecular species in supercritical fluids. In: D Fraser (ed) Thermodynamics in geology. Reidel, Boston, pp 161–181

Johannes W, Metz P (1968) Experimentelle Bestimmung von Gleichgewichtsbeziehungen im System $MgO-CO_2-H_2O$. N Jb Mineral Monatsh 112:15–26

Kerrick DM, Jacobs GK (1981) A modified Redlich-Kwong equation for H_2O, CO_2 mixtures at elevated pressures and temperatures. Am J Sci 281:735–767

Ohnmacht W (1974) Petrogenesis of carbonate orthopyroxenites (sagvandites) and related rocks from Troms, Northern Norway. J Petrol 15:303–323

Peretti A (1988) Occurrence and stabilities of opaque minerals in the Malenco serpentinite (Sondrio, Northern Italy). Ph D Thesis ETH Zurich No 8740

Pfeifer HR (1979) Fluid-Gesteins-Interaktion in metamorphen Ultramafititen der Zentralalpen. Ph D Thesis ETH Zurich No 6379

Philipp R (1988) Phasenbeziehungen in System $MgO-H_2O-CO_2-NaCl$. Ph D Thesis ETH Zurich No 8641

Philipp R, Girsperger S (1989) Experimental determination of phase transitions in the system $MgO-H_2O-CO_2$ using a pressure-analysis method. Contrib Mineral Petrol (in review)

Schramke JA, Kerrick DM, Blencoe JG (1982) The experimental determination of the brucite = periclase + water equilibrium with a new volumetric technique. Am Mineral 67:269–276

Schreyer W, Ohnmacht W, Mannchen J (1972) Carbonate orthopyroxenites (sagvandites from Troms, Northern Norway). Lithos 5:345–364

Skippen GB (1971) Experimental data for reactions in siliceous marbles. J Geol 79:457–481

Skippen GB (1974) An experimental model for low pressure metamorphism of siliceous dolomitic marble. Am J Sci 274:487–509

Skippen GB, Hutcheon I (1974) The experimental calibration of continuous reactions in siliceous carbonate rocks. Can Mineral 12:327–333

Skippen GB, Trommsdorff V (1986) The influence of NaCl and KCl on phase relations in metamorphosed carbonate rocks. Am J Sci 286:81–104

Trommsdorff V, Evans BW (1974) Alpine metamorphism of peridotitic rocks. Schweiz Mineral Petrogr Mitt 56:79–93

Trommsdorff V, Evans BW (1972) Progressive metamorphism of antigorite schist in the Bergell tonalite aureole. Am J Sci 272:423–437

Trommsdorff V, Evans BW (1977a) Antigorite-Ophicarbonates: Contact metamorphism in Valmalenco, Italy. Contrib Mineral Petrol 62:301–312

Trommsdorff V, Evans BW (1977b) Antigorite-Ophicarbonates: Phase relations in a portion of the system $CaO-MgO-SiO_2-H_2O-CO_2$. Contrib Mineral Petrol 60:39–56

Received July 4, 1989 / Accepted September 11, 1989
Editorial responsibility: J. Hoefs